An infinite element for analysis of transient fluid–structure interactions

Lorraine G. Olson and Klaus-Jürgen Bathe
Department of Mechanical Engineering, Massachusetts Institute of Technology, Cambridge, MA 02139, USA
(*Received July 1985*)

ABSTRACT

An infinite element based on the doubly asymptotic approximation (DAA) for use in finite element analysis of fluid–structure interactions is presented. Fluid finite elements model the region near the solid. Infinite elements account for the effects of the outer fluid on the inner region. The DAA-based infinite elements involve an approximate calculation of the added mass using static mapped infinite elements, plus a consistent damping term. Simple test analyses for a range of fluid properties demonstrate the performance of the solution technique. The analyses of a Helmholtz resonator (open pipe) and a circular plate in water indicate the practical use of the solution approach.

INTRODUCTION

Fluid–structure interactions affect many systems of industrial importance, and as a result much effort has gone into the development of finite element techniques for coupled fluid–solid systems. In numerous applications, such as offshore structures under earthquake loading, machinery vibrating in air, or pressure waves striking submarines, the fluid may be modelled as inviscid, irrotational, and *of infinite extent*. Modelling a sufficiently large region of fluid becomes too expensive for extended time analyses, and alternative approaches must be found.

From an engineering point of view, we would like to have a method which gives 'good' solutions for direct time integration, with the possibility of extending the method to include resonant frequency analyses. In addition, the method should fit the structure of general finite element codes, result in symmetric coefficient matrices, and should not increase the matrix bandwidths significantly.

Many approaches have been explored. Zienkiewicz *et al.*[1] review various methods. Mei[2] reviews techniques applied to water waves. We briefly discuss two of the major approaches below.

One widely used approach involves transforming the transient problem to the frequency domain. The infinite elements developed by Bettess and Zienkiewicz[3] fall into this category, since the assumed shape functions include a wave-like behaviour at a particular frequency. Astley[4] introduced wave envelope elements which also have inherent frequency dependence, but give better far field predictions. Boundary element or integral formulations, such as those developed by Wilton[5], Aranha *et al.*[6], or Zienkiewicz *et al.*[7] typically involve solutions in the frequency domain. If the transient solution is desired, however, a frequency solution is not necessarily the most straightforward approach.

Another frequently used approach is based on the use of the doubly asymptotic approximation (DAA). In this technique, the infinite fluid is modelled as the sum of two effects—the plane wave approximation at high frequencies and the added mass approximation at low frequencies. Felippa[8] rigorously derives the DAA and higher-order approximations (DAA2 and others) from Kirchhoff's retarded potential formulation. Geers[9] developes the DAA for fluid–structure interactions and Underwood and Geers[10] explore its use for soil–structure interactions. Vasudevan and DiMaggio[11] compare the DAA and DAA2 with other approximations. Zilliacus[12] implemented the DAA in the finite element code ADINA. These workers used the DAA to replace the entire infinite fluid region. Based on their experience with the DAA applied at the solid boundary, Nielson *et al.*[13] suggested using the DAA as a boundary condition on a small region of fluid near the structure.

We chose to apply the DAA as infinite elements which model the fluid far from the structure, while using finite elements near the solid. For the plane wave portion of the DAA we develop a consistent damping matrix. The added mass is approximated by *static* 'mapped infinite elements'. (Bettess and Bettess[14] give an excellent review of the extensive research in static infinite elements, and we refer to their paper for a detailed discussion of the origins of these elements.) This DAA infinite element approach may be used for direct time integration of dynamic response. It affects matrix bandwidth very little, and in the solution may simply be considered as a new element type.

In the next section of the paper we present the governing continuum mechanics equations that we use, followed by the corresponding finite element matrix equations. Sample solutions using the infinite element are given later. These numerical studies demonstrate the applicability of our solution approach.

GOVERNING EQUATIONS

Figure 1 shows the general fluid–structure interaction geometry. Solid extends throughout region S. The fluid region F represents the portion of the fluid which will be explicitly modelled, while the outer region O contains fluid which will be modelled using the doubly asymptotic approximation. The interface between the inner and outer fluid regions is denoted by E, while the fluid–structure interface region is I.

Solid

As discussed in our earlier paper[15], the principle of virtual displacements for the solid region is:

$$\int \bar{\boldsymbol{\varepsilon}}^{\mathrm{T}}\mathbf{C}_s\boldsymbol{\varepsilon}\,\mathrm{d}S + \int \rho\bar{\mathbf{u}}^{\mathrm{T}}\ddot{\mathbf{u}}\,\mathrm{d}S = \int \bar{\mathbf{u}}^{\mathrm{I}\mathrm{T}}\mathbf{f}^{\mathrm{I}}\,\mathrm{d}I \qquad (1)$$

where $\boldsymbol{\varepsilon}$ = strain tensor,
$\mathbf{C}_s$ = material stress–strain matrix,
ρ = density of solid,
$\mathbf{u}$ = displacement vector,
$\mathbf{f}^{\mathrm{I}}$ = surface (interface) force vector,
$\bar{x}$ = virtual x (e.g. virtual strain).

At the fluid–structure interface (I), the surface forces consist of externally applied forces ($\mathbf{f}^{\mathrm{A}}$) and forces due to

0264–4401/85/040319–11$2.00

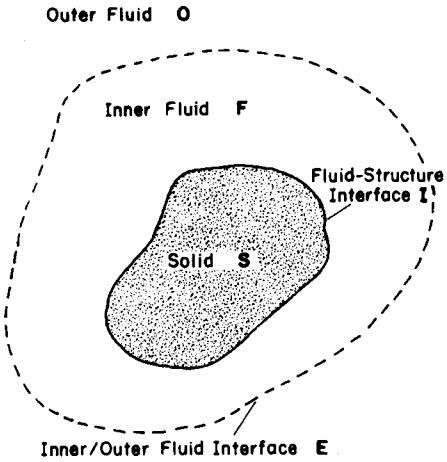

Figure 1 General fluid–structure interaction geometry

the fluid ($\mathbf{f}^F$). The fluid forces arise due to the pressure in the fluid. Expressing the fluid pressure in terms of the fluid velocity potential (ϕ) gives:

$$\mathbf{f}^F = \mathbf{n}\rho_F \dot{\phi}^I \tag{2}$$

where $\mathbf{n}^T = [n_x n_y n_z]$
$=$ unit outward normal from solid,
$\rho_F =$ density of fluid.

Substituting (2) into (1) produces:

$$\int \bar{\varepsilon}^T \mathbf{C}_s \varepsilon \, dS + \int \rho \bar{\mathbf{u}}^T \ddot{\mathbf{u}} \, dS = \int \bar{\mathbf{u}}^{IT} \mathbf{f}^A \, dI + \int \rho_F \bar{\mathbf{u}}^{IT} \mathbf{n} \dot{\phi}^I \, dI \tag{3}$$

which is the governing virtual work equation for the solid.

Fluid

The 'principle of virtual potentials' for the finite fluid region may be expressed as[15]:

$$\int \frac{1}{\beta} \bar{P}_0 P_0 \, dF - \int \frac{\rho_F}{\beta} \bar{P}_0 \dot{\phi} \, dF + \int \frac{\rho_F}{\beta} \bar{\phi} \dot{P}_0 \, dF - \int \frac{\rho_F^2}{\beta} \bar{\phi} \ddot{\phi} \, dF - \int \rho_F \mathbf{v} \bar{\phi} \cdot \mathbf{v} \phi \, dF = \int \bar{P}_0 u_N \, dI + \int \rho_F \bar{\phi}^I \dot{u}_N \, dI + \int \rho_F \bar{\phi}^E \frac{\partial \phi^E}{\partial n} \, dE \tag{4}$$

where $P_0 =$ hydrostatic pressure in the fluid
$\beta =$ bulk modulus of fluid,
$u_N =$ normal displacement at fluid boundary.

We note that the effect of the infinite fluid region has been introduced as the boundary condition of prescribed velocity on the boundary E (just as for the boundary condition on the solid–fluid interface I). The surface normal points into the finite fluid volume. For a bounded fluid region, we would retain the hydrostatic pressure variable. However, the hydrostatic pressure in an infinite fluid region cannot change, hence we can set P_0 to zero in (4) without loss of generality. In addition, the normal displacement of the fluid boundary must match the normal displacement of the solid at the fluid–structure interface, so that $u_N = \mathbf{n}^T \mathbf{u}^I$. This gives:

$$-\int \frac{\rho_F^2}{\beta} \bar{\phi} \ddot{\phi} \, dF - \int \rho_F \mathbf{v} \bar{\phi} \cdot \mathbf{v} \phi \, dF = \int \rho_F \bar{\phi}^I \mathbf{n}^T \dot{\mathbf{u}}^I \, dI + \int \rho_F \bar{\phi}^E \frac{\partial \phi^E}{\partial n} \, dE \tag{5}$$

We model the behaviour of the outer fluid region using the doubly asymptotic approximation. We can write:

$$\int \frac{\rho_F^2}{\beta} \bar{\phi} \ddot{\phi} \, dO + \int \rho_F \mathbf{v} \bar{\phi} \cdot \mathbf{v} \phi \, dO = \int \rho_F \bar{\phi}^E \frac{\partial \phi^E}{\partial n} \, dE \tag{6}$$

where we note that the normal points *out* of region O, *into* region F. In the low frequency limit, we have only the added mass effect,

$$\int \rho_F \mathbf{v} \bar{\phi} \cdot \mathbf{v} \phi \, dO = \int \rho_F \bar{\phi}^E \frac{\partial \phi^E}{\partial n} \, dE \tag{7}$$

Although the integration over O covers an infinite region, the value of the integral is finite (since it represents the kinetic energy in the fluid). In the high frequency limit, we make the plane wave approximation:

$$\frac{\partial \phi^E}{\partial t} = \sqrt{\frac{\beta}{\rho_F}} \frac{\partial \phi^E}{\partial n} \tag{8}$$

where $\sqrt{\beta/\rho_F}$ is the speed of sound in the fluid. This yields:

$$\int \sqrt{\frac{\rho_F^3}{\beta}} \bar{\phi}^E \dot{\phi}^E \, dE = \int \rho_F \bar{\phi}^E \frac{\partial \phi^E}{\partial n} \, dE \tag{9}$$

In the doubly asymptotic approximation, we superimpose these two effects to find:

$$\int \rho_F \mathbf{v} \bar{\phi} \cdot \mathbf{v} \phi \, dO + \int \sqrt{\frac{\rho_F^3}{\beta}} \bar{\phi}^E \dot{\phi}^E \, dE = \int \rho_F \bar{\phi}^E \frac{\partial \phi^E}{\partial n} \, dE \tag{10}$$

Finally, we substitute this expression for the surface integral (over E) into (5) to give:

$$-\int \frac{\rho_F^2}{\beta} \bar{\phi} \ddot{\phi} \, dF - \int \sqrt{\frac{\rho_F^3}{\beta}} \bar{\phi}^E \dot{\phi}^E \, dE - \int \rho_F \mathbf{v} \bar{\phi} \cdot \mathbf{v} \phi \, dF - \int \rho_F \mathbf{v} \bar{\phi} \cdot \mathbf{v} \phi \, dO = \int \rho_F \bar{\phi}^I \mathbf{n}^T \dot{\mathbf{u}}^I \, dI \tag{11}$$

Equation (11) forms the virtual work expression for the fluid.

FINITE ELEMENT DISCRETIZATION

Figure 2 shows the finite element discretization of the problem. The solid is modelled using ordinary solid finite elements, while the fluid is modelled with potential-based fluid finite elements. At the interface between the fluid and the structure we have fluid–structure interface elements. For the outer fluid region, we form infinite elements.

Element matrices

As described in our previous paper[15], the element matrices for the solid finite elements ($\mathbf{K}_{SS}$ and $\mathbf{M}_{SS}$) are formed in the usual way. The fluid elements generate the matrices $\mathbf{K}_{FF}$ and $\mathbf{M}_{FF}$. Fluid–structure interface elements contribute the matrices $\mathbf{C}_{FS}$ (these are not damping matrices), which couple the fluid to the solid.

For the infinite elements (*Figure 3*) we must evaluate

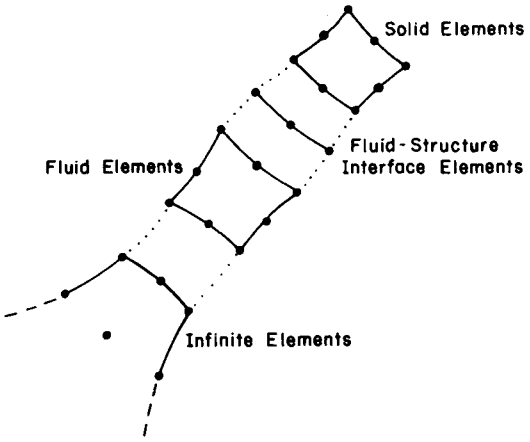

Figure 2 Finite element discretization

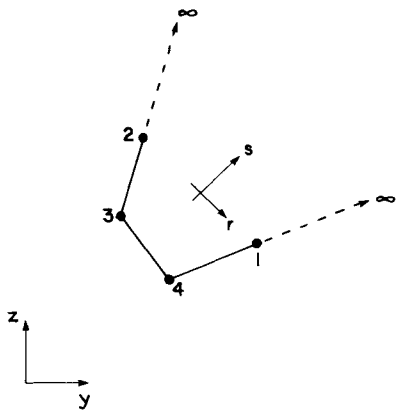

Figure 3 Typical two-dimensional infinite element

two terms, the damping term:

$$I_D = \int \sqrt{\frac{\rho_F^3}{\beta}}\, \bar{\phi}^E \dot{\phi}^E \, de \tag{12}$$

where de denotes integration over the element surface e (we now use lower case letters to denote element integrations) and the added mass term:

$$I_M = \int \rho_F \mathbf{v}\bar{\phi} \cdot \mathbf{v}\phi \, do \tag{13}$$

We derive the expressions for a typical 4-node two-dimensional infinite element below.

For the damping term we write:

$$y^E = \mathbf{H}\mathbf{y} \tag{14}$$

$$\mathbf{H} = [0\,0\,H_3\,H_4] \tag{15}$$

$$H_3 = (1-r)/2$$

$$H_4 = (1+r)/2$$

$$\mathbf{y}^T = [y_1\, y_2\, y_3\, y_4] \tag{16}$$

where $y^E = y$-coordinate of a point on the boundary E
$y_i = y$-coordinate of node i

Similarly,

$$z^E = \mathbf{H}\mathbf{z} \tag{17}$$

and

$$\phi^E = \mathbf{H}\boldsymbol{\phi} \tag{18}$$

This allows us to write:

$$\mathbf{C}_I = \int_{-1}^{1} \sqrt{\frac{\rho_F^3}{\beta}}\, \mathbf{H}^T\mathbf{H} \det \mathbf{J}^S \, dr \tag{19}$$

where $\det \mathbf{J}^S = \sqrt{(dy/dr)^2 + (dz/dr)^2}$ for the damping term. Note that the integration is over the boundary only.

We could evaluate the added mass in many ways, but we choose to use *static* 'mapped' infinite elements[14]. Within the infinite element, we use the interpolations (**h**) for the nodal point variable ϕ, but we use a different interpolation (**N**) for the nodal coordinates y and z. The nodal variable interpolations become:

$$\phi = \mathbf{h}\boldsymbol{\phi} \tag{20}$$

$$\mathbf{h} = [h_1\, h_2\, h_3\, h_4] \tag{21}$$

$$h_1 = H_4(1-s^2) \qquad h_2 = H_3(1-s^2)$$

$$h_3 = -H_3 s(1-s)/2 \qquad h_4 = -H_4 s(1-s)/2$$

Note that the nodal interpolations chosen imply that ϕ is zero at infinity (i.e. at $s = +1$). The coordinate interpolations for this particular element become:

$$y = \mathbf{N}\mathbf{y} \tag{22}$$

$$z = \mathbf{N}\mathbf{z} \tag{23}$$

$$\mathbf{N} = [N_1\, N_2\, N_3\, N_4] \tag{24}$$

$$N_1 = \left(\frac{1+s}{1-s}\right)H_4 \qquad N_2 = \left(\frac{1+s}{1-s}\right)H_3$$

$$N_3 = \left(\frac{-2s}{1-s}\right)H_3 \qquad N_4 = \left(\frac{-2s}{1-s}\right)H_4$$

These coordinate interpolations have the two key features that at any node i, $y = y_i$ and $z = z_i$ and that at $s = +1$, y and z go to infinity. Now we can write:

$$\mathbf{K}_I = \int_{-1}^{1}\int_{-1}^{1} \rho_F (\mathbf{J}^{-1}\mathbf{D}_L)^T (\mathbf{J}^{-1}\mathbf{D}_L) \det \mathbf{J} \, dr\, ds \tag{25}$$

where

$$\mathbf{D}_L = \begin{bmatrix} \frac{\partial h_1}{\partial r} & \frac{\partial h_2}{\partial r} & \frac{\partial h_3}{\partial r} & \frac{\partial h_4}{\partial r} \\ \frac{\partial h_1}{\partial s} & \frac{\partial h_2}{\partial s} & \frac{\partial h_3}{\partial s} & \frac{\partial h_4}{\partial s} \end{bmatrix}$$

and

$$\mathbf{J} = \begin{bmatrix} \frac{\partial y}{\partial r} & \frac{\partial z}{\partial r} \\ \frac{\partial y}{\partial s} & \frac{\partial z}{\partial s} \end{bmatrix}$$

The new coordinate interpolations **N** only affect **J**, and Gauss quadrature may be used to approximate the integral for $\mathbf{K}_I$.

Reference 14 gives more details about the derivation of these static infinite elements. One point must be emphasized here. The combination of the coordinate and nodal point variable interpolations is chosen so that:

$$\phi \approx a/l + b/l^2$$

where l is a decay length (and a and b are constants determined from the ϕ_i's). If we create an element which

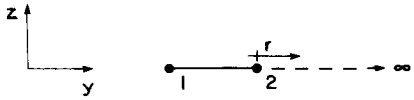

Figure 4 Infinite element with pure *y*-direction decay

decays only in the y direction (see *Figure 4*)

$$l \approx y - 2y_1 + y_2$$

We can adjust this length by adjusting the location of node 1 with respect to node 2. For a decay length $l = y$ we choose $y_2 = 2y_1$. Excellent results have been obtained using this static infinite element[14].

The same approach can be employed to implement six node two-dimensional elements with a parabolic interpolation in the r-direction, and three-dimensional elements which are infinite in the t-direction. We have implemented these elements in the program ADINA (version ADINA 84[16]).

Matrix equations

After assembling contributions from each type of element (i.e. solid, fluid–structure, finite fluid, and infinite fluid elements), we obtain the following matrix equations:

$$\begin{bmatrix} \mathbf{M}_{SS} & \mathbf{0} \\ \mathbf{0} & -\mathbf{M}_{FF} \end{bmatrix} \begin{bmatrix} \ddot{\mathbf{U}} \\ \ddot{\boldsymbol{\phi}} \end{bmatrix} + \begin{bmatrix} \mathbf{0} & \mathbf{C}_{FS}^{T} \\ \mathbf{C}_{FS} & -\mathbf{C}_{I} \end{bmatrix} \begin{bmatrix} \dot{\mathbf{U}} \\ \dot{\boldsymbol{\phi}} \end{bmatrix} + \begin{bmatrix} \mathbf{K}_{SS} & \mathbf{0} \\ \mathbf{0} & -\mathbf{K}_{FF} - \mathbf{K}_{I} \end{bmatrix} \begin{bmatrix} \mathbf{U} \\ \boldsymbol{\phi} \end{bmatrix} = \begin{bmatrix} \mathbf{R} \\ \mathbf{0} \end{bmatrix} \quad (26)$$

or

$$\mathbf{M}\ddot{\mathbf{X}} + \mathbf{C}\dot{\mathbf{X}} + \mathbf{K}\mathbf{X} = \mathbf{R} \quad (27)$$

This matrix equation occurs frequently in finite element analysis. We are using the Newmark method and the Wilson–θ method for the direct time integration[17]

EXAMPLE ANALYSES

In the examples which follow, we perform transient analyses of fluid–structure interactions for problems where the infinite extent of the fluid is important. In all cases, we have used the 6 node infinite element (for its superior resolution in the r-direction) with 3 point Gauss quadrature. The matrix equations were integrated in time using Newmark's method with $\delta = 0.5$ and $\alpha = 0.25$ (the trapezoidal rule).

Simple test cases—evaluating the DAA

For our small displacement analyses, the accuracy of the doubly asymptotic approximation depends on whether the pressure oscillations striking the infinite/finite element boundary are high-frequency waves, low-frequency waves, or intermediate frequency waves. We can express this using a dimensionless parameter[18]:

$$\eta = \omega l / c$$

where ω = characteristic frequency of motion of the solid,
l = characteristic length to boundary where DAA is applied,
c = speed of sound in fluid $= \sqrt{\beta/\rho_F}$

If η is large, the fluid behaves in a compressible manner and the plane wave approximation is valid. If η is small, the fluid behaves nearly incompressibly and the added mass effect dominates. In the 'in-between' region, we expect the worst performance using the doubly asymptotic approximation.

Figure 5 shows the four test cases designed at $\eta \approx 0.1$ ($\beta = 10^{10}$ N/m^2), $\eta \approx 1$ ($\beta = 10^8$ N/m^2) and $\eta \approx 10$ ($\beta = 10^6$ N/m^2), here $l = 1.0$ m, to examine the performance of the infinite/finite element technique using the DAA. *Figure 6* shows the mesh used for all four cases. Axisymmetric elements generate the two spherical geometries and plane elements give the cylindrical geometries. For the sphere/cylinder which oscillates as a rigid body we constrain the fluid–structure interface nodes to have the vertical displacement of node 3, while for the breathing sphere/cylinder cases we constrain the fluid–structure interface nodes to have displacements normal to the structure equal to the vertical displacement of node 3. Notice that, in each case, the sphere/cylinder has a characteristic mass and stiffness which gives it a resonant frequency in vacuum of 316 rad/s.

In case one, we examine the sphere 'breathing' in the infinite fluid, subject to a step in internal pressure at time zero (the net force over the entire sphere is 10^6 N). We vary the bulk modulus (β) to verify the doubly asymptotic

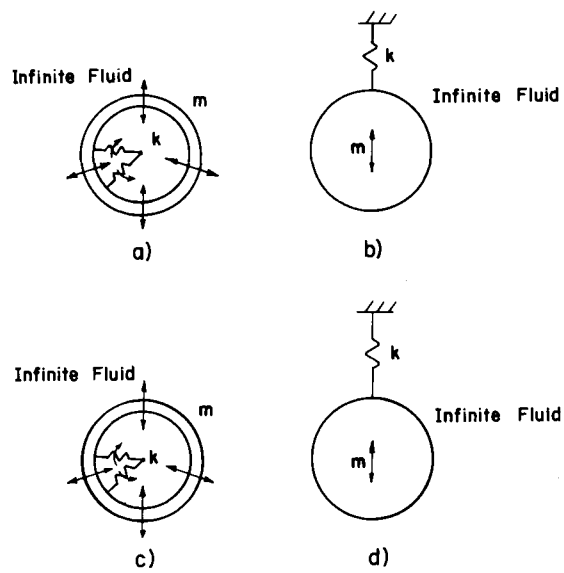

Figure 5 Four test cases: (a) sphere breathing; (b) sphere oscillating; (c) cylinder breathing; (d) cylinder oscillating

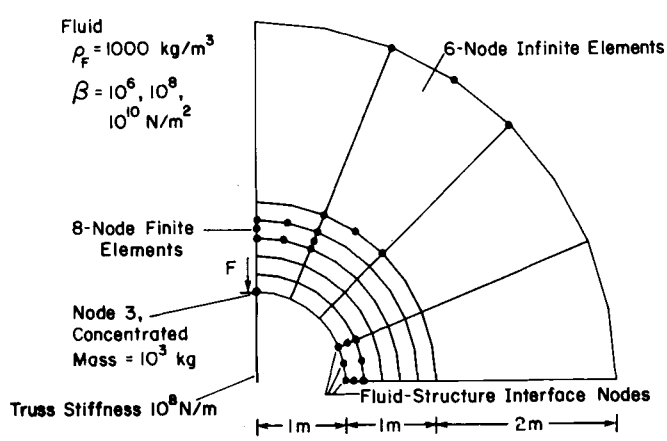

Figure 6 Mesh used for four test cases

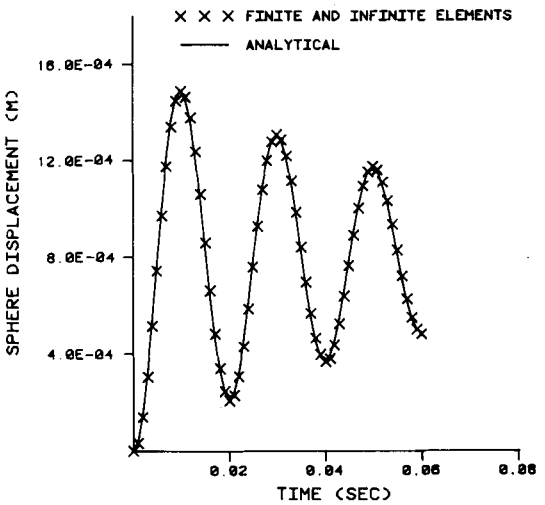

Figure 7a Sphere breathing. $\beta = 10^6$

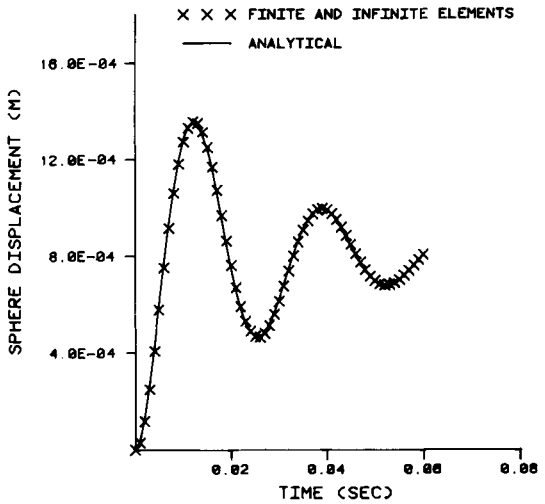

Figure 7b Sphere breathing. $\beta = 10^8$

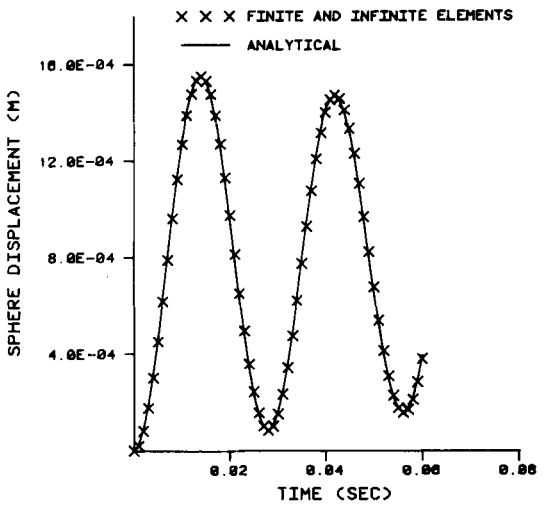

Figure 7c Sphere breathing. $\beta = 10^{10}$

nature of the solution. As shown in *Figure 7*, however, the solution for the sphere displacement appears to be exact for all three values of β. Appendix A shows that a very simple infinite/finite element model gives exactly the same characteristic equation as the analytical solution for this particular problem, regardless of the properties of the fluid or the solid.

For case two, we test the rigid sphere oscillating on a spring in an infinite fluid. At time zero, we apply a step force to the sphere (total force 10^6 N). Once again, we vary β and plot the analytical (see Appendix B) and infinite/finite element results. This time (see *Figure 8*) the results

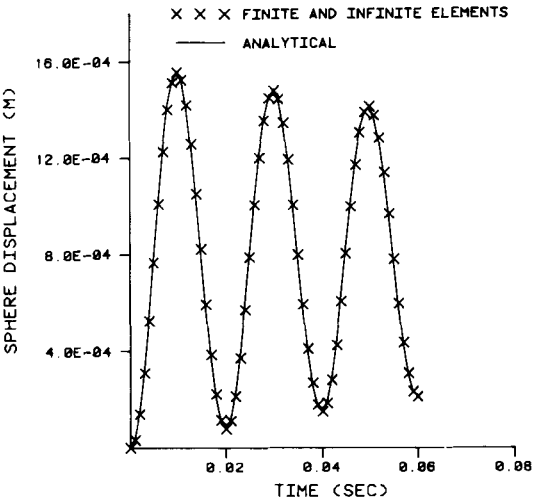

Figure 8a Sphere oscillating. $\beta = 10^6$

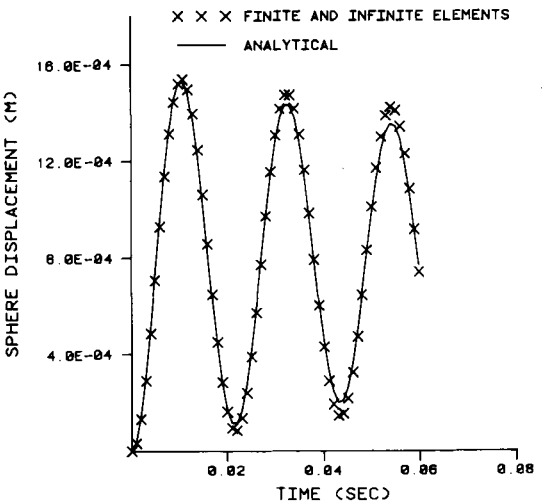

Figure 8b Sphere oscillating. $\beta = 10^8$

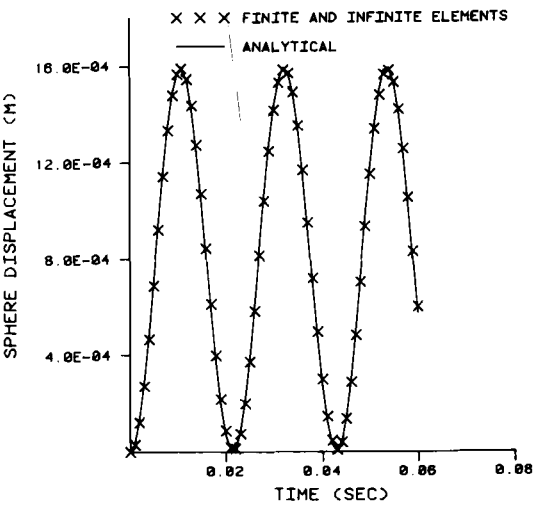

Figure 8c Sphere oscillating. $\beta = 10^{10}$

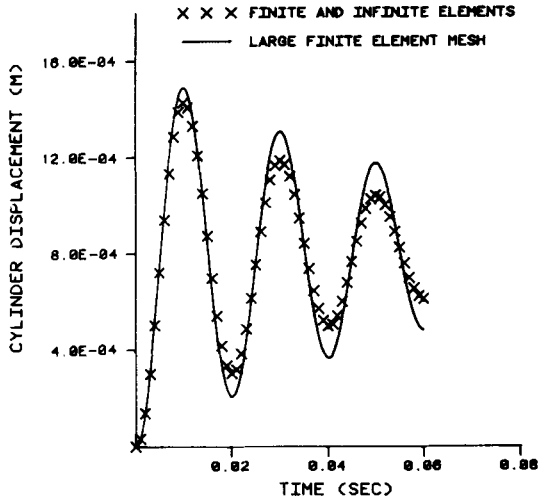

Figure 9a Cylinder breathing. $\beta = 10^6$

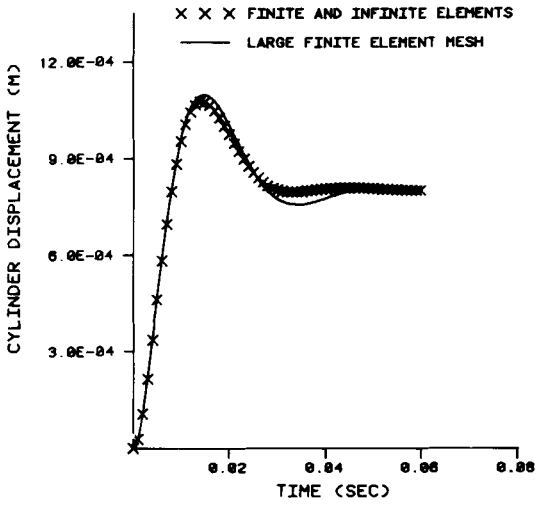

Figure 9b Cylinder breathing. $\beta = 10^8$

are excellent for the cases $\beta = 10^6$ and $\beta = 10^{10}$, and good for $\beta = 10^8$.

The third test case consists of a cylinder breathing in an infinite fluid. At time zero, a step in internal pressure is applied (total force $10^6/\pi$ N). Here we do not present an analytical solution, but instead compare with numerical solutions using large finite element meshes. We only consider the cases $\beta = 10^6$ and 10^8 N/m^2 because of the large fluid region affected by pressure waves in the case of $\beta = 10^{10}$ N/m^2. The finite element mesh for $\beta = 10^6$ N/m^2 extends 4 m in the radial direction, while the mesh for $\beta = 10^8$ N/m^2 has a radius of 22 m. Both meshes are large enough that the wave will not reach the edge of the domain during the analysis time. The finite element meshes have five 8-node elements/m in the radial direction and four elements in the circumferential direction, which gives the same number of elements/radial distance as the finite portion of the infinite/finite element mesh in *Figure 6*. *Figures 9a* and *9b* compare the infinite/finite element solutions with the finite element solutions.

Finally, we test the infinitely long cylinder oscillating as a rigid body in an infinite fluid, subject to a step in total force of $10^6/\pi$ N. *Figures 10a* and *10b* show the infinite/finite element and finite element solutions for $\beta = 10^6$ and 10^8 N/m^2. The same large finite element meshes as in test case 3 were used. *Figure 10c* compares the infinite/finite element solution for the large bulk modulus ($\beta = 10^{10}$ N/m^2) with the analytical incompressible fluid solution. In this last solution the frequency agreement is good. Damping does not exist in the analytical incompressible solution, although finite damping will occur for any finite bulk modulus.

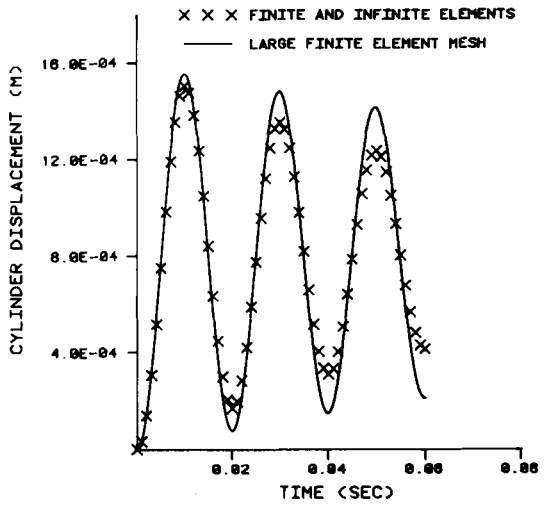

Figure 10a Cylinder oscillating. $\beta = 10^6$

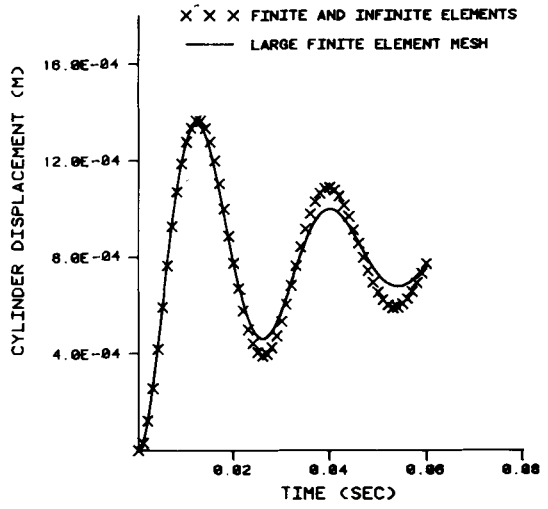

Figure 10b Cylinder oscillating. $\beta = 10^8$

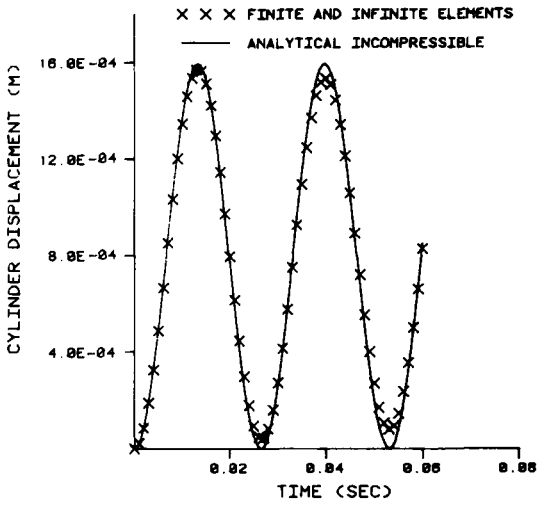

Figure 10c Cylinder oscillating. $\beta = 10^{10}$

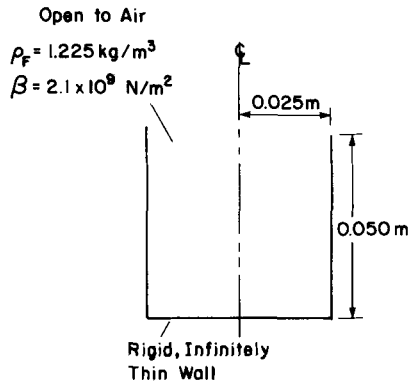

Figure 11 Open pipe geometry

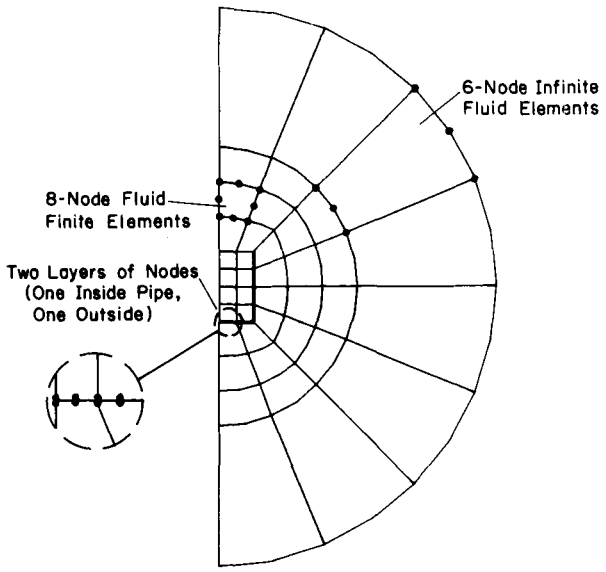

Figure 12 Infinite/finite element mesh for analysis of open pipe

For both cylinder test cases, a comparison of the solutions obtained with the large finite element meshes and the infinite/finite element meshes shows good correlation in the predicted oscillation periods. The damping predicted in the solutions shown in *Figures 9a*, *10a* and *10b* does not compare well, with the damping in the infinite/finite element solutions being larger or smaller.

Helmholtz resonator

To demonstrate the solution of a practical problem using infinite/finite element techniques, we chose to analyse a simple Helmholtz resonator. *Figure 11* shows the geometry considered: a short rigid pipe open at one end and closed at the other end. Alster[19] has investigated the effect of the air outside the pipe on the resonant frequencies of the system. Neglecting the outside air gives an analytical frequency of 1700 Hz, while experimentally Alster finds the first resonance at 1380 Hz.

Figure 12 shows the infinite/finite element mesh used to analyse the pipe. We calculate the time response resulting from an initial velocity potential of $\cos(\pi z/2L)$ (where L = pipe height) inside the pipe, and a potential of zero outside the pipe. *Figure 13* shows the velocity potential at the centre of the pipe bottom *versus* time. *Figure 13* also shows the same analysis performed using a large finite element mesh (see *Figure 14*). We see that the infinite/finite element results reproduce the large finite element results well. Estimating the resonant frequency of the system from *Figure 13* gives a value of 1340 Hz ± 5%. This compares well with the experimental value of 1380 Hz.

To identify the effectiveness of the infinite elements, we analysed the time response of the finite element mesh shown in *Figure 15*. This is the same configuration as in the infinite/finite element mesh (*Figure 12*), but without the infinite elements on the boundary. *Figure 16* shows the velocity potential at the centre of the pipe bottom as a function of time. Clearly this approach does not produce a good estimate of the system response.

Plate in water

Another problem of practical interest involves a circular iron plate mounted (clamped) into an infinite wall and exposed on one side to water (*Figure 17*). Lamb[20] examined this same system and estimated the resonant frequency and damping rate based on a Rayleigh–Ritz analysis of the plate and water. For this geometry and material properties Lamb found a plate frequency in

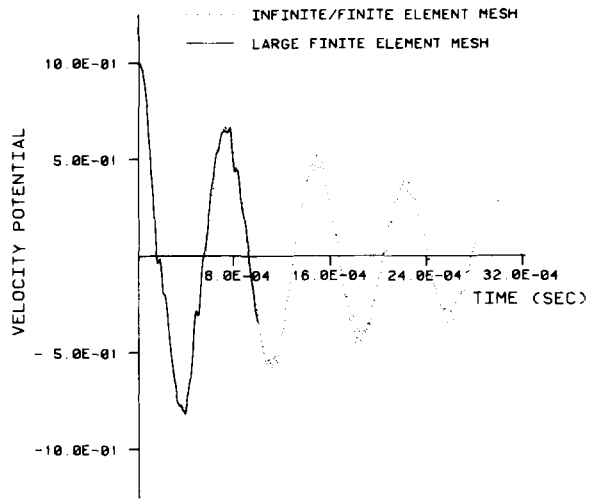

Figure 13 Transient response of open pipe

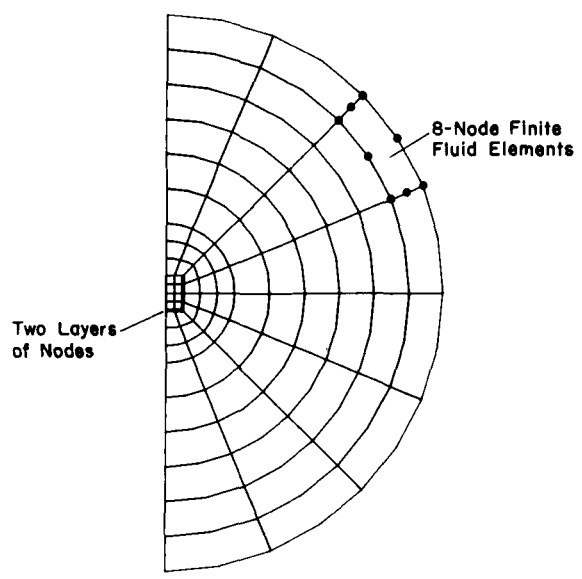

Figure 14 Large finite element mesh for analysis of open pipe

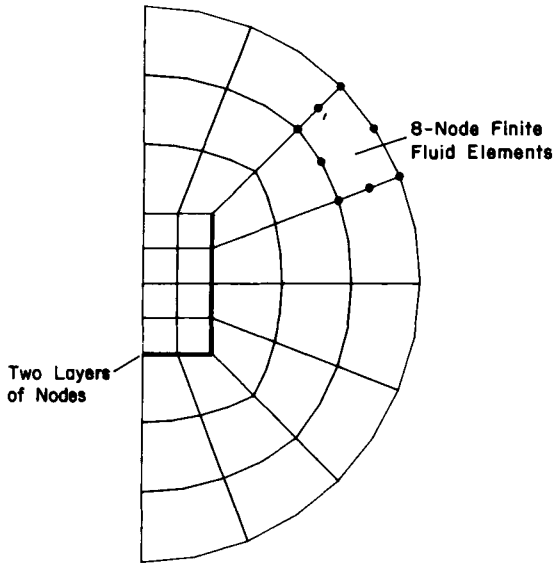

Figure 15 Small finite element mesh for analysis of open pipe

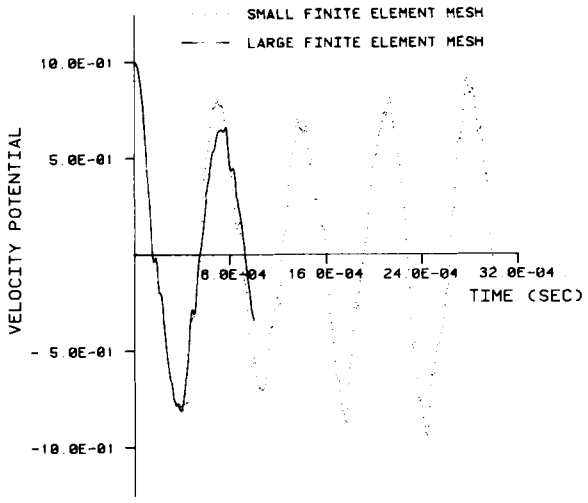

Figure 16 Transient response of open pipe. Study of small finite element mesh results

vacuum of 1013 Hz, a plate frequency in water of 550 Hz ($\omega = 3456$ rad/s), and a displacement decay of $\exp(-t/\tau)$ where $\tau = 0.0094$ s.

Figure 18 shows the mesh used to analyse the plate in vacuum. We find a fundamental frequency of 1005 Hz, which agrees well with Lamb's result.

For the plate in water, we first used the mesh shown in *Figure 19*. We give the plate an initial displacement corresponding to its first mode of vibration in vacuum, and apply zero velocity potential in the fluid. *Figure 20* shows the displacement of the centre of the wetted surface of the plate as a function of time. *Figure 20* also shows a curve derived from Lamb's analysis of the form:

$$\delta = B\cos(\omega t)\,e^{-t/\tau}$$

where δ is the plate displacement (and B is the initial value). The two curves agree quite well, both in damping rate and frequency.

Figure 21 shows a mesh which uses only infinite elements in the fluid. *Figure 22* compares the time response of this system to Lamb's analysis. In this case, when we omit the fluid finite elements near the structure, the infinite elements introduce too much damping and increase the frequency. This suggests that it is, in fact, better to model the region near the solid with finite elements and treat the far region with infinite elements.

Finally, *Figure 23* shows another choice for the infinite/finite element mesh. Once again we achieve good results for the transient response, as shown in *Figure 24*. This indicates that the response of the infinite/finite element system is relatively insensitive to mesh selection, so long as the mesh chosen is reasonable.

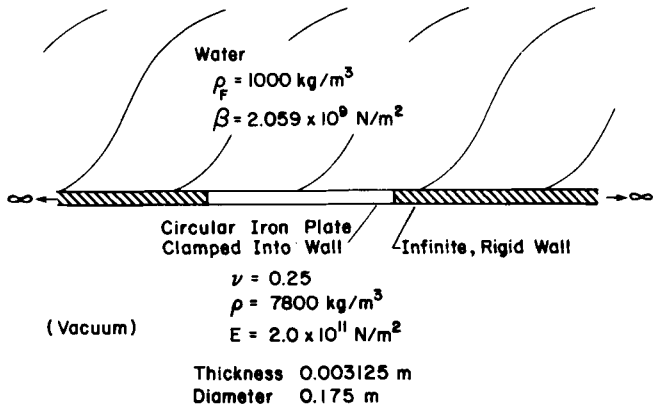

Figure 17 Circular plate in water

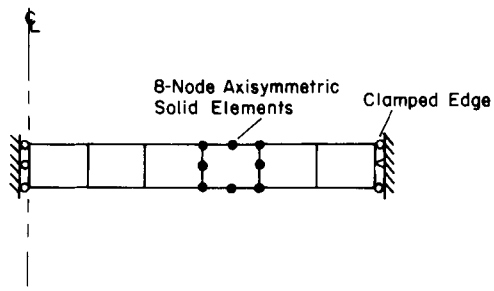

Figure 18 Finite element mesh for analysis of plate in vacuum

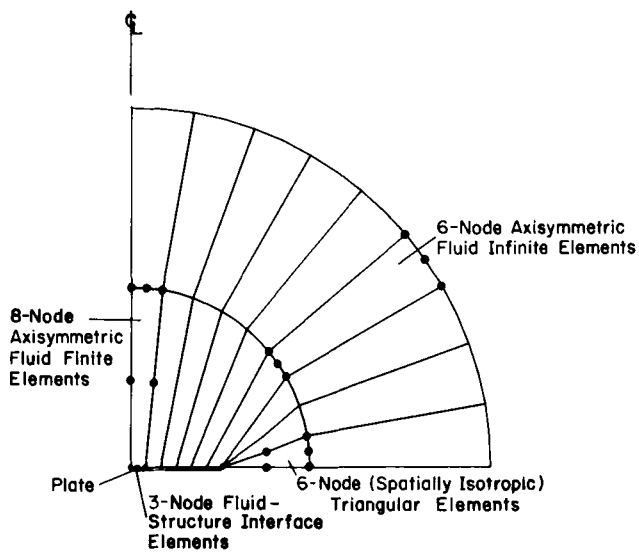

Figure 19 Infinite/finite element mesh for analysis of plate in water

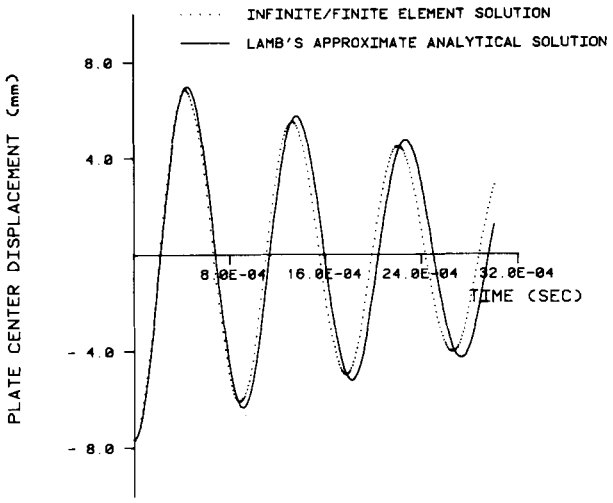

Figure 20 Transient response of plate in water

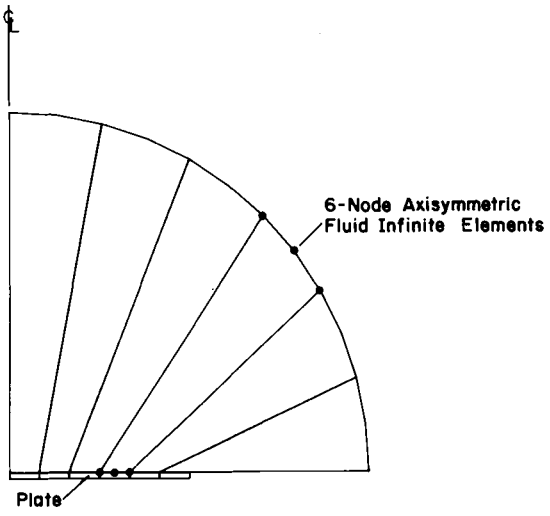

Figure 21 Infinite element mesh for analysis of plate in water

CONCLUSIONS

We have introduced a new implementation of the doubly asymptotic approximation (DAA) for use in analysing fluid–structure interactions. Fluid finite elements model the region near the structure. To model the effect of the far field on the fluid finite elements, we introduce 'infinite elements' based on the DAA. This involves an approximate calculation of the added mass using static infinite elements. Consistent damping matrices account for the plane wave approximation in the DAA.

We chose this approach for several reasons. A number of researchers have explored the DAA and concluded that the DAA represents an effective approximation for a range of fluid–structure problems. With the approach of modelling the region near the solid with finite elements, we can also obtain good resolution near difficult contours. From an implementation point of view we simply introduce another element group into ADINA for the infinite elements. The infinite elements do not increase the bandwidth of the matrix equations significantly, and the governing matrix equations remain symmetric and can be directly integrated in time for transient analyses.

The simple analyses of a sphere and a cylinder vibrating in a fluid given in this paper show excellent results for the sphere. In the analyses of the cylinder, the vibration periods are well predicted but the damping does not compare well with the results obtained using standard large finite element meshes. The solution of a simple Helmholtz resonator shows good agreement between the numerical and available experimental results. Finally,

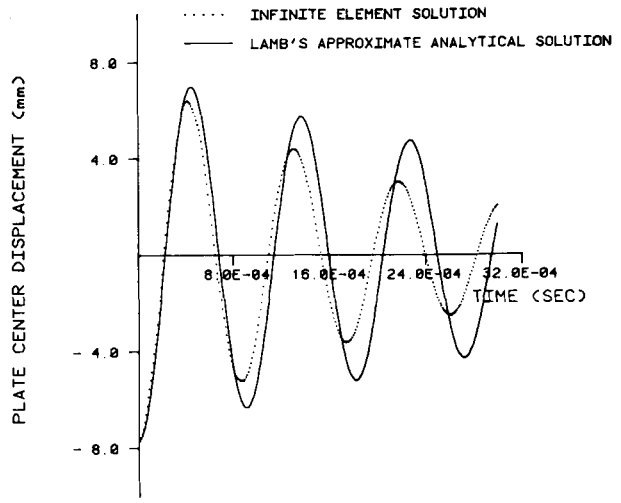

Figure 22 Transient response of plate in water. Study of infinite element mesh results

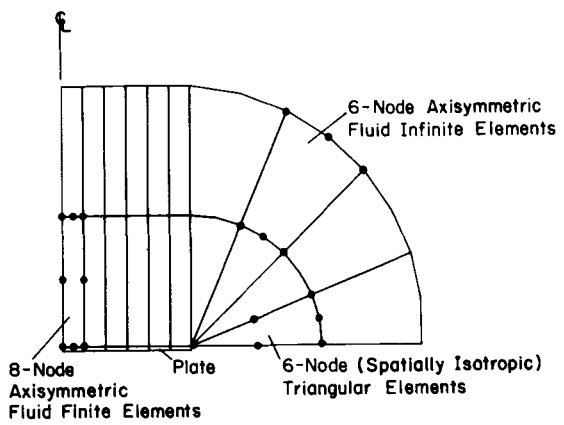

Figure 23 Another infinite/finite element mesh for analysis of plate in water

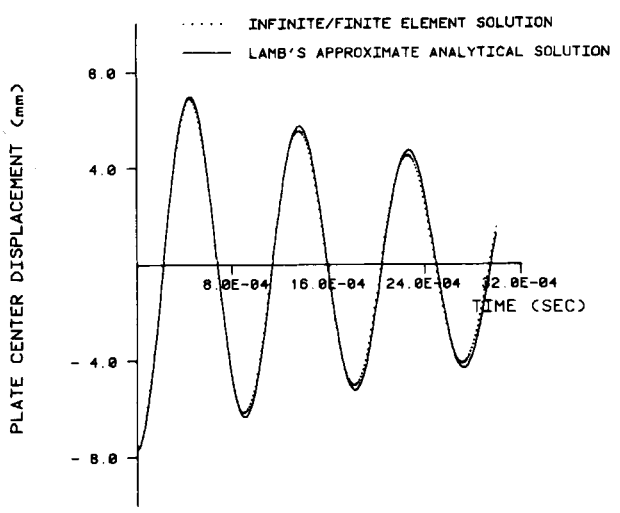

Figure 24 Transient response of plate in water using mesh of *Figure 23*

infinite/finite element solutions for the frequency and damping of a circular plate in water compare favourably with an approximate analytical solution.

The proposed technique represents a valuable solution approach for a variety of problems. However, further studies are desirable regarding various items in the formulation: the accuracy with which the damping of fluid–structure systems is predicted, the use of different order expansions in the infinite elements, the modelling of the fluid motion in the infinite region with more sophisticated approximations (e.g. the use of the DAA2 could be explored), and the application of the solution technique to more complex geometries. In this research, the test case of the cylinder should be further studied to obtain more insight into the response of the system and the effect of the various assumptions. Finally, research into establishing an effective eigenvalue solution technique for the matrix equations derived would be valuable.

ACKNOWLEDGEMENTS

We are grateful for the financial support of ADINA Engineering AB, Sweden, and of the Forschungszentrum GKSS, West Germany, through Mr. R. Dietrich, for this work. We also thank International Business Machines Corporation for providing financial support for Lorraine Olson.

REFERENCES

1 Zienkiewicz, O. C., Kelley, D. W. and Bettess, P. The Sommerfeld (radiation) condition of infinite domains and its modelling in numerical procedures, *Lecture Notes in Mathematics*, Vol. 704, Springer-Verlag, Heidelberg (1979)
2 Mei, C. C. Numerical methods in water–wave diffraction and radiation, *A. Rev. Fluid Mech.*, **10**, 393–416 (1978)
3 Bettess, P. and Zienkiewicz, O. C. Diffraction and refraction of surface waves using finite and infinite elements, *Int. J. Num. Method. Eng.*, **11**, 1271–1290 (1979)
4 Astley, R. J. Wave envelope and infinite elements for acoustical radiation, *Int. J. Num. Method. Fluids*, **3**, 507–526 (1983)
5 Wilton, D. T. Acoustic radiation and scattering from elastic structures, *Int. J. Num. Method. Eng.*, **13**, 123–138 (1978)
6 Aranha, J. A., Mei, C. C. and Yue, D. K. P. Some properties of a hybrid element method for water waves, *Int. J. Num. Meth. Eng.*, **14**, 1627–1641 (1979)
7 Zienkiewicz, O. C., Kelley, D. W. and Bettess, P. The coupling of the finite element method and boundary solution procedures, *Int. J. Num. Method. Eng.*, **11**, 355–375 (1977)
8 Felippa, C. A. Top-down derivation of doubly asymptotic approximations for structure–fluid interaction analysis, *Innovative Numerical Analysis for the Applied Engineering Sciences*, The University Press of Virginia (1980)
9 Geers, T. L. Doubly asymptotic approximations for transient motions of submerged structures, *J. Acoust. Soc. Am.*, **64**, 1500–1508 (1978)
10 Underwood, P. and Geers, T. L. Doubly asymptotic, boundary element analysis of dynamic soil–structure interaction, *Int. J. Solids Struct.*, **17**, 687–697 (1981)
11 Vasudevan, R. and DiMaggio, F. Transient response of submerged shells using improved acoustic approximations, *Comput. Struct.*, **14**, 187–194 (1981)
12 Zilliacus, S. Fluid–structure interaction and ADINA, *Comput. Struct.*, **17**, 763–773 (1983)
13 Neilson, H. C., Everstine, G. C. and Wang, Y. F. Transient response of a submerged fluid-coupled double-walled shell structure to a pressure pulse, *J. Acoust. Soc. Am.*, **70**, 1776–1782 (1981)
14 Bettess, P. and Bettess, J. A. Infinite elements for static problems, *Eng. Comput.*, **1**, 4–16 (1984)
15 Olson, L. G. and Bathe, K. J. Analysis of fluid–structure interactions. A direct symmetric coupled formulation based on the fluid velocity potential, *Comput. Struct.*, **21**, 21–32 (1985)
16 *ADINA (Automatic Dynamic Incremental Nonlinear Analysis) User's Manual*, Report AE 84-1, ADINA Engineering, Watertown, MA and Vasteras, Sweden (December 1984)
17 Bathe, K. J. *Finite Element Procedures in Engineering Analysis*, Prentice-Hall, Englewood Cliffs, NJ (1982)
18 Batchelor, G. K. *An Introduction to Fluid Dynamics*, Cambridge University Press, New York (1981)
19 Alster, M. Improved calculation of resonant frequencies of Helmholtz resonators, *J. Sound Vib.*, **24**, 64–85 (1972)
20 Lamb, H. On the vibrations of an elastic plate in contact with water, *Proc. R. Soc. (A)*, **98**, 205–216 (1921)
21 Lamb, H. *Hydrodynamics*, 6th Edn, Dover, New York (1945)

APPENDIX A—SPHERE BREATHING

Analytical solution

The motion of the sphere and the fluid is purely radial in the case of a 'breathing' sphere, and the wave equation for the fluid reduces to:

$$\frac{1}{r^2}\frac{\partial}{\partial r}\left(r^2\frac{\partial\phi}{\partial r}\right)=\frac{1}{c^2}\frac{\partial^2\phi}{\partial t^2} \tag{28}$$

where r = radial coordinate and t = time. Let Φ be the Laplace transform of ϕ so that:

$$\frac{1}{r^2}\frac{\partial}{\partial r}\left(r^2\frac{\partial\Phi}{\partial r}\right)=\frac{s^2}{c^2}\Phi \tag{29}$$

(ϕ and $\dot{\phi}$ are initially zero) which has the solution:

$$\Phi=A_1\frac{e^{(sr/c)}}{r}+A_2\frac{e^{-(sr/c)}}{r} \tag{30}$$

Since we want only outgoing waves, $A_1=0$ and

$$\Phi=A_2\frac{e^{-(sr/c)}}{r} \tag{31}$$

At $r=a$ (the sphere radius), we know that:

$$\frac{\partial\Phi}{\partial r}=sX=A_2\left(\frac{-sa}{c}e^{-(sa/c)}-e^{-(sa/c)}\right)\frac{1}{a^2} \tag{32}$$

where X is the Laplace transform of the radial sphere displacement. Solving for the coefficient A_2 yields:

$$A_2=\frac{-a^2sX\,e^{(sa/c)}}{(1+sa/c)} \tag{33}$$

so that:

$$\Phi|_a=\frac{-asX}{(1+sa/c)} \tag{34}$$

The governing equation for the sphere in the fluid is:

$$s^2mX+kX=F+\rho_F s\Phi|_a(4\pi a^2) \tag{35}$$

Here, F is the Laplace transform of the total applied force (pressure times area), and $\rho_F s\Phi$ represents the fluid pressure loading. The stiffness and mass of the sphere in vacuum are k and m, respectively. Substituting from (34) gives:

$$F=s^2mX+kX+\frac{\rho_F s^2}{(1+sa/c)}4\pi a^3X \tag{36}$$

or

$$\frac{F}{X}=k\left(\frac{1+s\left(\frac{a}{c}\right)+s^2\left(\frac{m}{k}+\frac{\rho_F 4\pi a^3}{k}\right)+s^3\left(\frac{ma}{kc}\right)}{1+s\frac{a}{c}}\right) \tag{37}$$

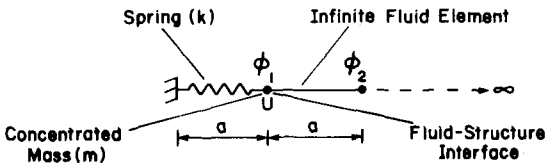

Figure 25 Simple infinite/finite element model of breathing sphere

We find the solution for a step in applied force (pressure) using the inverse Laplace transform.

Finite element solution

We propose a simplified finite element model for this problem which has only three degrees of freedom (see *Figure 25*). The governing matrix equation becomes:

$$\begin{bmatrix} m & 0 \\ 0 & 0 \end{bmatrix}\begin{bmatrix} \ddot{U} \\ \ddot{\phi}_1 \end{bmatrix}+\begin{bmatrix} 0 & C_{FS} \\ C_{FS} & -C_I \end{bmatrix}\begin{bmatrix} \dot{U} \\ \dot{\phi}_1 \end{bmatrix}+\begin{bmatrix} k & 0 \\ 0 & -K_{EFF} \end{bmatrix}\begin{bmatrix} U \\ \phi_1 \end{bmatrix}=\begin{bmatrix} f \\ 0 \end{bmatrix} \tag{38}$$

where $K_{EFF}=(K_{11}K_{22}-K_{12}K_{12})/K_{22}$ is the effective stiffness of the two node infinite element.

Evaluating the **C** matrix gives $C_{FS}=-4\pi a^2\rho_F$ and $C_I=4\pi a^2\rho_F/c$ (both act over the total surface area of the sphere). Exact integration of the **K** matrix for the (spherical) infinite element yields:

$$\mathbf{K}_I=\tfrac{4}{3}\rho_F\pi a\begin{bmatrix} 7 & -8 \\ -8 & 16 \end{bmatrix}$$

so that $K_{EFF}=4\rho_F\pi a$.

Performing the Laplace transformation of the matrix (38) produces:

$$\begin{bmatrix} k+s^2m & sC_{FS} \\ sC_{FS} & -K_{EFF}-sC_I \end{bmatrix}\begin{bmatrix} X \\ \Phi \end{bmatrix}=\begin{bmatrix} F \\ 0 \end{bmatrix} \tag{39}$$

or

$$\frac{F}{X}=k\left(\frac{1+s\dfrac{C_I}{K_{EFF}}+s^2\left(\dfrac{m}{k}+\dfrac{C_{FS}^2}{kK_{EFF}}\right)+s^3\dfrac{m}{k}\dfrac{C_I}{K_{EFF}}}{1+s\dfrac{C_I}{K_{EFF}}}\right) \tag{40}$$

With the values given previously,

$$C_I/K_{EFF}=a/c$$

$$C_{FS}^2/K_{EFF}=4\pi a^3\rho_F$$

which gives exactly the same result as the analytical solution.

APPENDIX B—SPHERE OSCILLATING

Analytical solution

For outgoing waves, the solution which satisfies the wave equation and the boundary condition at the sphere is[21]:

$$\Phi=A_1\frac{e^{-sr/c}}{r^2}\left(\frac{sr}{c}+1\right)\cos\theta \tag{41}$$

where

$$A_1=\frac{-sXa^3e^{sa/c}}{\left(2+2\dfrac{sa}{c}+\dfrac{s^2a^2}{c^2}\right)} \tag{42}$$

This gives:

$$\Phi|_a=-sXa\frac{\left(\dfrac{sa}{c}+1\right)\cos\theta}{\left(2+2\dfrac{sa}{c}+\dfrac{s^2a^2}{c^2}\right)} \tag{43}$$

For the sphere in water, the governing equation becomes:

$$s^2mX+kX=F+\int\rho_F s\Phi\cos\theta\,dA \tag{44}$$

or

$$s^2mX+s^2m'X\frac{\left(\dfrac{sa}{c}+1\right)}{\left(1+\dfrac{sa}{c}+\dfrac{1}{2}\dfrac{s^2a^2}{c^2}\right)}+kX=F \tag{45}$$

where $m'=(2/3)\rho_F\pi a^3$ (the added mass for the incompressible fluid limit). Rewriting gives:

$$\frac{F}{X}=k\left\{\frac{1+s\left(\dfrac{a}{c}\right)+s^2\left(\dfrac{m}{k}+\dfrac{1}{2}\dfrac{a^2}{c^2}+\dfrac{m'}{k}\right)+s^3\left(\dfrac{ma}{kc}+\dfrac{m'a}{kc}\right)+s^4\left(\dfrac{ma^2}{2kc^2}\right)}{1-s\left(\dfrac{a}{c}\right)+s^2\left(\dfrac{1}{2}\dfrac{a^2}{c^2}\right)}\right\} \tag{46}$$

We find the solution for a step in force by using the inverse Laplace transform on (46).